



Cite This: ACS Cent. Sci. XXXX, XXX, XXX-XXX

Research Article http://pubs.acs.org/journal/acsci

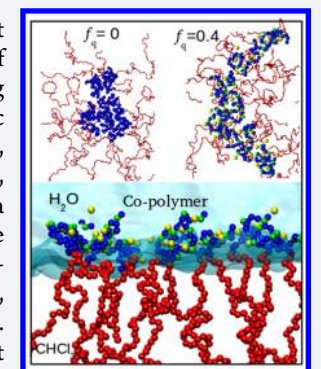
Self-Assembly of Charge-Containing Copolymers at the Liquid— **Liquid Interface**

Felipe Jiménez-Ángeles, †, Lo Ha-Kyung Kwon, Kazi Sadman, Thomas Wu, Kenneth R. Shull, Gand Monica Olvera de la Cruz*, †, ‡, \$, \$

[†]Department of Materials Science and Engineering, [‡]Department of Chemistry, [§]Department of Chemical and Biological Engineering, and Department of Physics, Northwestern University, Evanston, Illinois 60208, United States

Supporting Information

ABSTRACT: Quantitatively understanding the self-assembly of amphiphilic macromolecules at liquid-liquid interfaces is a fundamental scientific concern due to its relevance to a broad range of applications including bottom-up nanopatterning, protein encapsulation, oil recovery, drug delivery, and other technologies. Elucidating the mechanisms that drive assembly of amphiphilic macromolecules at liquid—liquid interfaces is challenging due to the combination of hydrophobic, hydrophilic, and Coulomb interactions, which require consideration of the dielectric mismatch, solvation effects, ionic correlations, and entropic factors. Here we investigate the self-assembly of a model block copolymer with various charge fractions at the chloroform-water interface. We analyze the adsorption and conformation of poly(styrene)-block-poly(2-vinylpyridine) (PS-b-P2VP) and of the homopolymer poly(2-vinylpyridine) (P2VP) with varying charge fraction, which is controlled via a quaternization reaction and distributed randomly along the backbone. Interfacial tension measurements show that the polymer adsorption increases only marginally at low charge fractions (<5%) but increases more significantly at higher charge fractions for the



copolymer, while the corresponding randomly charged P2VP homopolymer analogues display much more sensitivity to the presence of charged groups. Molecular dynamics (MD) simulations of the experimental systems reveal that the diblock copolymer (PS-b-P2VP) interfacial activity could be mediated by the formation of a rich set of complex interfacial copolymer aggregates. Circular domains to elongated stripes are observed in the simulations at the water-chloroform interface as the charge fraction increases. These structures are shown to resemble the spherical and cylindrical helicoid structures observed in bulk chloroform as the charge fraction increases. The self-assembly of charge-containing copolymers is found to be driven by the association of the charged component in the hydrophilic block, with the hydrophobic segments extending away from the hydrophilic cores into the chloroform phase.

INTRODUCTION

Copolymers with amphiphilic properties can be used in a wide range of applications including thin-film nanopatterning, 1-3 bottom-up nanofabrication, 4-7 demulsifying and antifoaming in extraction methods, 8-10 drug delivery, 11 and protein encapsulation. 12,13 In bulk water conditions, the solvation and dissociation of charged macromolecules favors solubilization, unless multivalent ions¹⁴ or oppositely charged macroions15 are added in the system, and dominates the assembly of charged containing copolymers in low monovalent salt conditions. 16 In organic media, on the other hand, ionic correlations in charge-containing copolymers lead to the formation of ionic clusters. 18-22 The ionic clusters can lead to nontrivial thermodynamic changes in the molten state, such as the evolution of inverted phases, 6,23 and ion-dependent miscibility of ion-conducting block copolymers.²⁴ Theoretical developments have identified the effects of ion-ion correlations, 25-29 solvation energy of ions, 30-33 and translational entropy of ions as significant influences on determining the thermodynamics of charge-containing copolymers. The combination of these effects are unknown in amphiphilic

charge-containing copolymers at the interface between organic solvents and water.

The Langmuir-Blodgett technique has been used to analyze thin-films of a variety of block copolymer structures at airwater interfaces, including extended planar domains, hexagonal and square 2D patterns of dotlike structures, stripes, nanowires, and nanorods.^{34–47} Like in the bulk, the phase behavior of block copolymers at air-water interfaces is governed by the hydrophilic to hydrophobic length ratio. 17,34,35,47 Unfortunately, the Langmuir—Blodgett technique is very difficult to utilize at liquid-liquid interfaces. Here we investigate the assembly of a model amphiphilic copolymer at the interface of an organic solvent and water as a function of the fraction of charged groups in the copolymer by using a combination of interfacial tension measurements and molecular dynamics (MD) simulations. Amphiphilic charged block copolymers are usually described by means of the charge fraction f_q and the hydrophilic fraction f_a . Here we investigate the effect of varying both parameters $f_{\rm q}$ and $f_{\rm a}$ in the adsorption

Received: January 25, 2019



Figure 1. (a) Schematic setup for measuring the interfacial tension. The drop deformation is indicative of changes in the surface tension. The interfacial tension is calculated by fitting the drop profile and determining the shape parameter B_0 and radius of curvature R_0 , which are related to the interfacial tension, γ , via eq 1. (b) Reaction scheme for quaternizing poly(2-vinylpyridine) with bromoethane. Here we can define the charge fraction $f_q = N_{q2vp} / (N_{2vp} + N_{q2vp})$ and the hydrophilic fraction $f_a = (N_{q2vp} + N_{2vp}) / (N_s + N_{2vp} + N_{q2vp})$. We further define the total number of hydrophilic groups as $N_{hp} = N_{q2vp} + N_{2vp}$, where N_{q2vp} and N_{2vp} are the number of 2VP and Q2VP monomers, respectively. We should note, however, that the 2VP monomers preserve some hydrophobic character.

and assembly in partially quaternized polystyrene-block-poly(2-vinylpyridine) (PS-b-P2VP) at the water—chloroform interface (see Figure 1).

The PS and P2VP blocks can be synthesized using anionic polymerization allowing us to control the hydrophilic fraction f_a . Furthermore, the P2VP block can be selectively quaternized allowing control over the charge fraction f_{α} along the block without relying on pH-dependent ionization. The MD simulations are used to investigate the effects of charge on the self-assembly, partitioning, and adsorption to liquid-liquid interfaces including ionic correlations, ion solvation, and van der Waals interactions. These experimentally guided MD simulations can also propose possible structures/conformations of the polymers at the interface as a function of polymer amphiphilicity. An interfacial tension measurement lacks interfacial structural details and does not provide the concentration of adsorbed molecules, allowing simulations to synergistically provide this information by using the measured tension as input. Previous research on PS-b-P2VP has shown that the micellar self-assembly of these block copolymers is dependent on the quaternizing agent,³⁷ the selection of solvent or ionic liquid, 3,7,48 and the block length and hydrophilicity of each block. 49 Several works to date have employed modification of the P2VP block to introduce charge into the backbone, noting that this makes the block copolymer extremely sensitive to water, unlike the unmodified versions. The current view of PS-b-P2VP self-assembly at the air-water interface portrays the copolymer aggregation through the hydrophobic blocks whereas the hydrophilic segments extend into the aqueous phase due to their mutual electrostatic repulsion. 39,40,47 That view, however, does not take account ionic correlations and the dielectric variations at the interface. We demonstrate here that these two factors play a fundamental role in the copolymer self-assembly at the interface.

Here, by combining experimental measurements and molecular simulations, we investigate the effect of charge fraction and hydrophilic fraction on the self-assembly of PS-b-P2VP at the chloroform—water interface to reveal the copolymer self-assembly mechanisms. We use the pendant drop shape method in our experimental studies of the liquid—liquid interface. MD simulations are employed to unveil the

self-assembly details of systems. Atomic-scale simulations of macromolecular systems are limited to take into account the difference in length and time scales for the macromolecules and the individual solvent molecules. Ocarse-grain simulation schemes are used here to span molecular simulations to longer time and length scales. We use the MARTINI force-field, which consistently maps to some atomistic details and has been used to simulate systems of large molecules like biomolecules, surfactants, and polymers. The paper we discuss the experimental and simulation results followed by discussion and conclusions, with experimental and simulation details provided at the end of the paper.

■ RESULTS AND DISCUSSION

Interfacial tension, as measured by drop shape apparatus, is a very useful method for determining the interfacial behavior of block ionomers. Interfacial tension was measured by extracting the drop profile in time increments and fitting it to the Laplace equation (eq 1) as described in Figure 1. It is to be noted that the Laplace equation describes a balance between the surface tension γ , which tries to keep the spherical shape of the drop, and the density difference, which tries to pull the drop in an upward direction. A deformation of the drop, as shown in Figure 1, is indicative of changes in the interfacial tension, and is tracked by extracting the drop profile and fitting R_0 , the radius of curvature at the apex, and R_0 , the shape parameter, to calculate the interfacial tension γ . In eq 1, $\Delta \rho$ is the difference in densities of the two liquids, and g is the gravity acceleration.

$$B_0 = \frac{\Delta \rho g R_0^2}{\gamma} \tag{1}$$

The interfacial tension measurements show that an increase in charge fraction is correlated with a significant drop in the interfacial tension at the chloroform—water interface (see Figure 2). This is due to increased adsorption of the block copolymers at the water—chloroform interface with increasing charge fraction. The difference is insignificant from $f_{\rm q}=0$ to

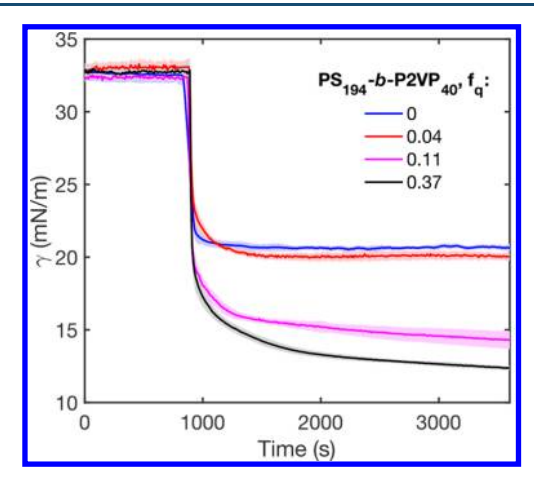


Figure 2. Interfacial tension of the diblock copolymer PS-b-P2VP at chloroform—water interface and at different charge fractions, $f_{\rm q}$ (degree of quaternization), for the P2VP block. The block copolymer is constituted by $N_{\rm s}=194$ styrene monomer and $N_{\rm hp}=40$ hydrophilic monomers ($f_{\rm a}=0.17$), where $N_{\rm hp}=N_{\rm 2vp}+N_{\rm q2vp}$ and $N_{\rm 2vp}$ and $N_{\rm q2vp}$ are the number of 2VP and Q2VP units, respectively. The pristine water—chloroform tension is measured for 900 s to ensure absence of contaminants, before polymer injection into the chloroform phase resulting in adsorption. A substantial drop in interfacial tension is seen for all samples. Error bars are reported as the standard deviation of three measurements. Solution pH was mildly acidic due to carbonic acid buildup under ambient conditions; therefore the P2VP units were assumed to be partially charged (p $K_{\rm a}$ P2VP ≈ 5).

0.04, but is nonmonotonic and larger in magnitude with subsequent increases in copolymer's charge fraction.

It is now important to comment on the pH responsiveness of P2VP, and consider some experimental nuances before comparison with simulations. Quaternizing P2VP with bromoethane using the scheme shown in Figure 1b results in permanent strong charges that are dissociated in water at all pH. However, the remaining pyridine units have a p $K_a \approx 5$, which is not far from ambient pH.65 In all experiments described here, Milli-Q water was used to eliminate contamination. We did not utilize buffers since they result in significant complexity in terms of buffer capacity, valency of buffer ions, buffer-polymer interactions, ionic strength, and the introduction of an extra contamination source. These factors would introduce more complexities in performing the experimental measurements. While the absence of buffer reduces system complexity, it adds an important consideration: the degree of quaternization, f_q , is the minimum average charge on the hydrophilic block. This is due to the fact that Milli-Q water turns mildly acidic (pH 6-7) under ambient exposure to air from carbonic acid formation. It follows that some P2VP units will become ionized due to its weakly basic character, bringing the effective charge to be always greater than f_q . Since carbonic acid has a p $K_a \approx 6.4$, the pH of water will become weakly buffered around this value. Using eq 2, we can calculate the approximate degree of ionization, α , of the P2VP blocks to be \approx 0.04, bringing that total effective charge to be $\approx f_{\rm q}$ + 0.04(1 - $f_{\rm q}$). Therefore, the pH induced ionization of P2VP is quite small, and we refer to the charge fraction as simply f_q in the remainder of the manuscript. We note that f_q is the measure of the charge fraction in the P2VP block. The hydrophilic fraction f_a comprehends the polar and charged units. The 2VP units are polar and they are more hydrophobic than the styrene monomers, nevertheless, 2VP preserve some

hydrophobic character. These 2VP units may also be protonated, in which case they become compleately hydrophilic. Here we refer to the 2VP units as the hydrophilic monomers.

$$pK_{a} = pH + \log\left(\frac{\alpha}{1 - \alpha}\right) \tag{2}$$

The primary reason for adsorption of molecules to the liquid—liquid interface is to decrease the incompatibility between the hydrophilic (hydrophobic) groups from the polymer and chloroform (water). This can be tested by analyzing the adsorption of the quaternized poly-2-vinyl-pyridine (P2VP) homopolymer at different charge fractions (see Figure 3). The difference in behavior between the

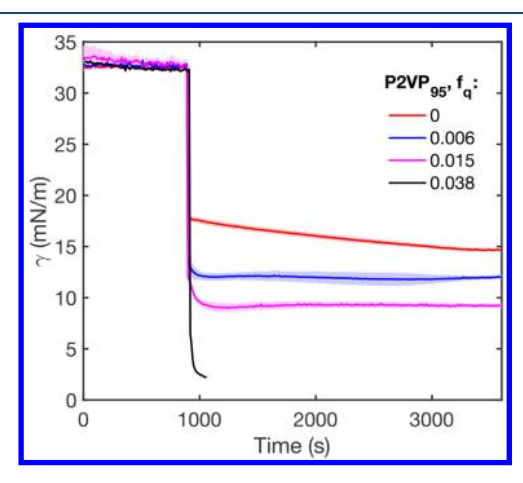


Figure 3. Interfacial tension of the partially and randomly quaternized P2VP homopolymer at chloroform—water interface and at different charge fractions, $f_{\rm q}$ (degree of quaternization). The polymer is made of 95 2VP monomers. Polymer was injected into the chloroform phase and allowed to adsorb to the water interface. At sufficiently large charge fractions, the polymer becomes more soluble in the aqueous phase, which lowers the tension to nearly zero.

homopolymer and the copolymer is due to the solubilization of the hydrophobic PS block in chloroform. In the case of PS-b-P2VP at the water-chloroform interface, increasing the charge fraction allows compatibilization of both water and chloroform phases by associating with water via the charge-carrying ends and associating with chloroform via the hydrophobic PS block. This argument follows that an increase in interfacial adsorption is correlated with the increase in hydrophilicity due to charge. However, this simple interpretation ignores important thermodynamic factors such as the competition among entropy, solvation of both charged groups in water and of the PS block in the chloroform, and the ionic correlations of the charged groups which when forced to be close to the chloroform phase are stronger due to the dielectric mismatch. Without a quantitative understanding of these competing parameters, the interfacial structure and concentration of adsorbates cannot be determined. For this, we turn to molecular dynamics simulations of interfacial adsorption, and find that an increase in charge in these block ionomers leads to a structural transition of the micelles similar to the transition observed in the pure chloroform phase when the charge fraction in the P2VP block increases.

The MD model setup and coarse-grain scheme are outlined in Figure 4, and further details of the simulation protocol are provided in the Materials and Methods section. In chloroform,

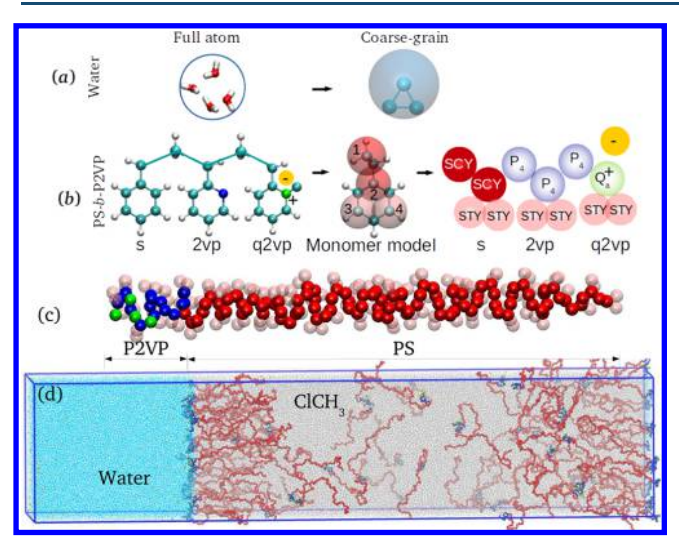


Figure 4. Models and simulation setup. (a) A cluster of four water molecules is mapped into a molecule constituted by three charged sites. (b) The monomers styrene (S), 2-vinylpyridine (2VP), and the quaternized 2-vinylpyridine (Q2VP) are represented by a four-bead model. (c) Copolymer constituted by $N_{\rm s}$ styrene (nonpolar) monomers, $N_{\rm hp}$ polar monomers ($N_{\rm 2vp}$ 2-vinyylpyridine monomers and $N_{\rm q2vp}$ quaternized 2-vinyylpyridine monomers). The degree of polymerization is given as $N_{\rm p}=N_{\rm s}+N_{\rm hp}=60$ in all our simulations; $N_{\rm hp}=N_{\rm 2vp}+N_{\rm q2vp}$. The hydrophilic and the charge fractions are given as $f_{\rm a}=N_{\rm hp}/N_{\rm p}$ and $f_{\rm q}=N_{\rm q2vp}/N_{\rm hp}$, respectively. (d) Water–chloroform (CHCl₃) interface with an amphiphilic copolymer. The bead color code is as follows: The polar (P₄) and the quaternized (Q_a) backbone groups in 2VP are in dark blue and green, respectively. The counterions are in yellow. The backbone groups in the PS block are colored in red (SCY). The ring groups are colored in pale pink (STY).

the dielectric constant is $\epsilon_{\rm r}=4.4$, which means that the energy of coupling between the ions is about $\approx-20k_{\rm B}T$, and at the interface there is a higher mean dielectric constant which reduces the ionic coupling to about $-10k_{\rm B}T$. This would suggest that the diblock copolymer should not adsorb to the interface. Of course, there are other entropic and enthalpic advantages for the block ionomer to move to the interface. One, as discussed above, is the decrease in incompatibility between polymer and the two liquid phases (water and chloroform). In addition, adsorbing the charge-carrying parts of the chain into the aqueous phase lowers the system free energy by solvation of the charged groups and increases the system entropy via ion dissociation, which can now move across the medium.

The water—chloroform interfacial tension from our simulations (without the polymer) is $\gamma \approx 28$ mN/m which is in agreement with a previous simulation study⁶⁶ and is in relatively good agreement with our experimental measurement of $\gamma \approx 32$ mN/m (see Figure 2). According to the Gibbs adsorption isotherm equation ($d\gamma = -\Sigma_i \Gamma_i d\mu_i$) the interfacial tension decreases by increasing the surface concentration of the components at the interfacial region (Γ_i), provided that $d\mu_i > 0$. The surface concentration of copolymers at the interface Γ_p is regulated by the polymer concentration in chloroform. In our MD simulations Γ_p is adjusted to match the interfacial tension measurements at each charge fraction. When the polymer adsorption is set to $\Gamma_p \approx 0.06$ molecules/nm² the interfacial tension from our MD simulations is $\gamma \approx 22$ mN/m at all the polymer charge fractions from $f_q = 0$ to 0.4. This

interfacial tension from MD is similar to the experimental value observed at $f_q = 0$ in Figure 2. By setting $\Gamma_p = 0.20$ molecules/ nm^2 and $f_q = 0.4$ the interfacial tension from MD simulations is $\gamma \approx 8$ mN/m which is comparable to the measured interfacial tension of $\gamma \approx 12$ mN/m at a polymer charge fraction of f_q = 0.37. This analysis shows that the copolymer adsorption in the experiments is significantly increased by increasing the polymer charge fraction. It should be pointed out that only the hydrophilic block (corresponding to about 1/6 of the copolymer) is adsorbed at the interface while the PS block remains dissolved in chloroform. The P2VP homopolymer contributes with more than double of adsorbed groups at the interface than the copolymer because the whole molecule is adsorbed. Hence, experimentally a homopolymer is more effectively adsorbed than a copolymer at a similar charge fraction. We will come back to this point when we discuss the homopolymer simulation results.

In our MD simulations the electrostatic interaction between two charged sites i and j is given by the Coulomb potential as $u_{ij}^{\mathrm{el}}(r) = \frac{q_i q_j}{4\pi\epsilon_0 \epsilon_i r};$ where i and j are two charged sites which can be from the water molecules, counterions, and quaternized groups; ϵ_0 is the vacuum permittivity; and ϵ_r is the dielectric permittivity of the uniform background in which the whole simulation box is embedded. The polarizable water model is parametrized using a uniform dielectric background with $\epsilon_{\rm r}$ = 2.5. Hence, an effective dielectric constant $\epsilon_{\rm eff}$ of about 80 is established in the aqueous phase⁶⁰ due to the polarizable water molecules combined with the uniform dielectric background. The dielectric permittivity in chloroform is equal to the dielectric constant of the uniform background of the simulation box, i.e., $\epsilon_{\rm eff}$ = 2.5 in the chloroform phase. These values are closely matched to the measured dielectric constants of 78.4 and 4.4 at room temperature for water and chloroform, respectively. 67,68 The interface is the region of approximately 2 nm where the water and chloroform meet resulting in an abrupt change of the density profiles of the two liquids. At the interface, the dielectric permittivity is expected to be lower than in bulk water but higher than in bulk chloroform. Our explicit liquids (water and chloroform) indeed create a dielectric mismatch at the interface by establishing a lower $\varepsilon_{\rm eff}$ in chloroform and at the interfacial region than in water. In consequence, the ion-ion and ion-quaternized group effective electrostatic interactions are stronger in chloroform and at the interfacial region than in bulk water.

The copolymer polar and charged groups drive the hydrophilic blocks from chloroform toward the waterchloroform interface. Our MD simulations show that the hydrophobic blocks stay untangled and extended into the liquid chloroform, while the hydrophilic blocks assemble at the interface. The assemblies' geometry depends on the copolymer charge fraction f_q and surface concentration Γ_p . Figure 5 shows typical configurations of the copolymer aggregates at the water-chloroform interface at different charge fractions. The polar segments of the uncharged polymers ($f_{\rm q}=0$) form aggregates of circular and irregular shape spread on the xyplane (see Figure 5a). A lateral view from the xz-plane shows that the uncharged polar groups are inside the chloroform phase close to the aqueous phase (see Figure 5b). At the polymer's charge fraction of $f_q = 0.2$ the hydrophilic segments at the interface are loosely packed and form elongated strips on the xy-plane (see Figure 5c); the polar chains slightly penetrate into the aqueous phase (see Figure 5d). At a polymer charge

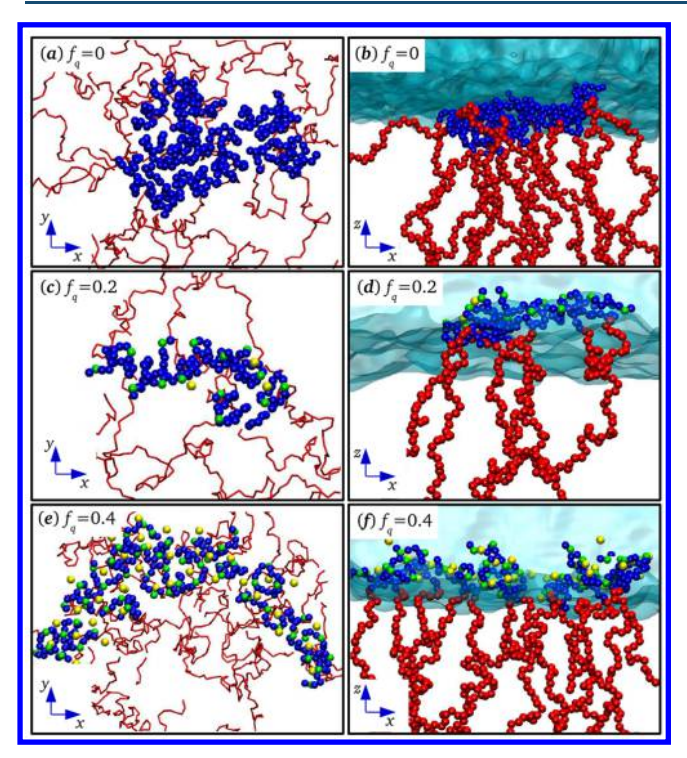


Figure 5. Top view from the *xy*-plane and lateral view from the *xz*-plane of the aggregates of copolymer PS-b-P2VP at the water—chloroform interface. The charge fraction and polymer interfacial adsorption are (a, b) $f_{\rm q}=0$ ($N_{\rm q2vp}=0$) and $\Gamma_{\rm p}=0.06$ molecules/nm²; (c, d) $f_{\rm q}=0.2$ ($N_{\rm q2vp}=2$) and $\Gamma_{\rm p}=0.06$ molecules/nm²; (e, f) $f_{\rm q}=0.4$ ($N_{\rm q2vp}=4$) and $\Gamma_{\rm p}=0.20$ molecules/nm². The polar groups and the quaternized groups in the P2VP block are in dark blue and green, respectively. The counterions are colored in yellow. The backbone groups in the PS block are colored in red. The ring groups in the PS block are not shown for clarity. The aqueous phase (snapshots from the *xz*-plane) is in transparent cyan, and the water surface is at one-half of the bulk density, approximately. $f_{\rm a}=0.16$ ($N_{\rm hp}=10$).

fraction of 0.4 the charged segments are densely packed and arrange into elongated strips (see Figure 5e). The end monomers of the hydrophilic segments are well inside the aqueous phase pulled by the quaternized Q_a groups (see Figure 5f). As the copolymer charge fraction f_q increases the hydrophilic blocks penetrate more into the aqueous phase. The density profiles demonstrate this effect (see Figure S5 in the Supporting Information). The interfacial tension decreases monotonically as a function of the number of adsorbed molecules at the interface (see Figure S6 in the Supporting Information), implying that there is no phase separation at these conditions.

MD simulations show that the ratio of bound counterions per Q_a groups at the interface increases from about 0.1 at f_q = 0.1 to 0.6 at $f_q = 0.4$ (see Figure S5 in the Supporting Information). Hence, at low charge fractions the electrostatic repulsion between the charged segments is not efficiently screened by the weakly bound counterions. At a low charge fraction the copolymer aggregation is driven by hydrophilichydrophobic forces that compete with the electrostatic repulsion. This competition reflects into the loosely packed aggregates. At high charge fractions the counterions are strongly bound to the charged block. Since the dielectric permittivity is higher at the interface than in chloroform the counterions can move between the quaternized groups. The strong binding makes the counterions and the quaternized Q groups form strongly correlated structures of intercalated charged groups. In these structures the electrostatic correlations dominate over the translational entropy of counterions. The radial distribution functions show a much stronger correlation between Q_a groups at $f_q = 0.4$ than at $f_q = 0.1$ (see Figure S7 in the Supporting Information), which is correlated with the higher adsorption of counterions at $f_q = 0.4$. This strong correlation between the copolymer and the counterions is sometimes referred to as "counterion condensation". 69,70 The correlations between the charged groups of the polymer and the counterions decrease the electrostatic

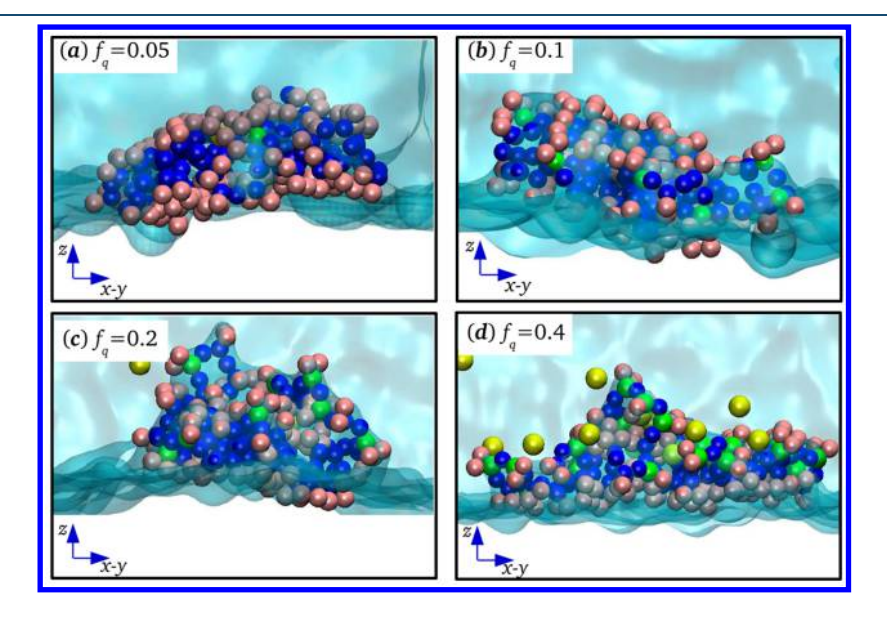


Figure 6. Lateral view of a homopolymer P2VP at the water—chloroform interface: (a) $f_q = 0.05$ ($N_{q2vp} = 3$); (b) $f_q = 0.1$ ($N_{q2vp} = 6$); (c) $f_q = 0.2$ ($N_{q2vp} = 12$); (d) $f_q = 0.4$ ($N_{q2vp} = 24$). The polar (P_4) and quaternized (Q_a) backbone groups are colored in dark blue and green, respectively. The ring groups (STY) are colored in pink. The counterions are colored in yellow. The aqueous phase is in transparent cyan, and the water surface is located at one-half of the bulk density, approximately. $f_a = 1$ ($N_{hp} = N_p = 60$).

repulsion between the charged blocks giving rise to densely packed aggregates.

To further investigate the self-assembly mechanisms we simulate a single partially quaternized homopolymer P2VP (randomly charged) at the water-chloroform interface. The polymer is initially placed into the chloroform phase, and during the simulation it is adsorbed at the water-chloroform interface (see Figures S8 and S9 and Movie S1 in the Supporting Information). It is interesting to see that in chloroform the counterions remain bound to the Q_a groups, and they are released into the aqueous phase when the polymer is adsorbed at the interface. The Qa-counterion binding is due to the electrostatic attraction. Hence, the counterion release into the aqueous phase demonstrates the change in the dielectric constant between the chloroform and the aqueous phase. As we pointed out above, the change from chloroform to the aqueous phase seems unfavorable because it implies a decrease of the electrostatic attraction (increase of energy). We will show that solvation energy makes the process favorable.

When the P2VP blocks are uncharged they aggregate to reduce the incompatibility between the hydrophilic/hydrophobic groups with chloroform—water. In chloroform, the nonpolar rings form a shell to reduce the contact between the polar groups (P_4) and the chloroform molecules. At the interface, the rings open up to allow the contact between the polar groups and water (see Figure S8d,e in the Supporting Information).

Experimentally, we observe that the randomly charged homopolymer of P2VP is much more sensitive to changes in the charge fraction than the homopolymer PS-b-P2VP. Due to the differences in the molecular weight and composition, the homopolymer has more than double the number of polar groups than the block copolymer per molecule. In addition, at the same charge fraction there are more than twice the Q groups in the homopolymer than the copolymer. Furthermore, the copolymer micellization in chloroform and the steric barrier created by the hydrophobic tail at the interface obstacle the adsorption of PS-b-P2VP. From all the aforementioned, the P2VP homopolymer adsorbs more effectively at lower charge ratios than the copolymer.

Figure 6 shows snapshots of a homopolymer P2VP adsorbed at the water-chloroform interface at the charge fractions of f_{q} = 0.05, 0.1, 0.2, and 0.4. At f_q = 0 the incompatibility between the polar groups and chloroform drives the polymer adsorption from the chloroform phase toward the interface. It is noteworthy that the polymer prefers the interface over the bulk aqueous phase even at the high charge fraction of $f_q = 0.4$. This can be rationalized by noting that significant hydrophobic character in the polymer is preserved in the pyridine groups. In our model, the polymer hydrophobicity is taken into account by means of the nonpolar ring atoms (STY). The MD simulations show that the polymer is held at the interface through the nonpolar ring groups (STY) remaining into the chloroform phase. The polar (P₄) and charged (Q₃) groups tend to be exposed to the aqueous phase. Some nonpolar ring groups are brought into the aqueous phase by the charged and polar groups. At lower charge fractions the polymer is located more into the chloroform phase (see Figures S8 and S9 in the Supporting Information). At the interface the polymer chain $(f_{\rm q} \leq 0.4)$ is folded into random coil configurations. The attraction between the nonpolar ring groups (STY) contributes significantly to the chain folding mechanism. The folding through the aggregation of the nonpolar groups minimizes the contact with water. At $f_{\rm q}=0.2$ some charged groups penetrate into the aqueous phase driven by the counterions which are diffusely distributed from the interfacial region and into the aqueous phase. Similar to the copolymer, as the charge fraction increases more counterions are bound to the polymer at the interface. The polymer—counterion binding decreases the electrostatic repulsion among the quaternized charged groups and aids the polymer chain folding by bridging the quaternized charged groups.

The systematic analysis of the polymer adsorption at the water–chloroform interface by increasing the hydrophilic fraction $f_{\rm a}$ and keeping constant the charge fraction $f_{\rm q}=0.2$ shows the formation of a two-dimensional percolated state (Figure S10 in the Supporting Information).

In our first set of experiments the randomly quaternized homopolymer was placed in chloroform and then allowed to adsorb to the water—chloroform interface (see Figure 3). At f_q = 0.038, the interfacial tension drops close to zero, suggesting that the polymer possesses enough charge to disrupt the water interface when adsorbing from chloroform. P2VP at very low f_q is insoluble in water and becomes insoluble in chloroform at high f_q . Now we demonstrate experimentally that at f_q = 0.038 the homopolymer can be adsorbed from both chloroform and water. We performed the inverse experiment by placing the P2VP homopolymer (f_q = 0.038) in water and then adsorbed onto the water—chloroform interface as shown in Figure 7. We

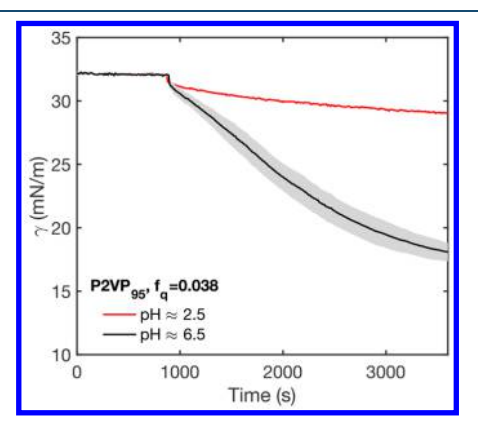


Figure 7. Adsorption of partially quaternized P2VP with $f_{\rm q}=0.038$ from water to a chloroform interface. At this charge ratio, P2VP became soluble in water, but the unquaternized units retained hydrophobic character, as observed from the adsorption to chloroform interface. However, under more acidic pH P2VP is expected to be fully protonated, and therefore to be hydrophilic. Thus, the adsorption is largely eliminated under acidic conditions.

observe that adsorption occurs at pH ≈ 6.5 where P2VP is slightly protonated. When the homopolymer is adsorbed from water the interfacial tension drops to about 17 mN/m (see Figure 7 at pH ≈ 6.5) whereas it drops to about 2 mN/m when adsorbed from chloroform (see Figure 3). In both cases the interfacial tension drop from the homopolymer is more pronounced than from the copolymer at a similar charge fraction ($\gamma \approx 20$ mN/m, see Figure 2 at $f_{\rm q}=0.04$). As explained above, this may be caused by a higher number of polar groups and charges per molecule in the homopolymer than in the copolymer. In the interfacial tension measurements the polymer adsorption is almost eliminated at pH ≈ 2.5 when most of the P2VP monomers are expected to be protonated,

giving the polymer highly cationic character. According to our MD simulations a polymer with charge fractions higher than $f_{\rm q}$ = 0.5 tends to be in the aqueous phase (see Figure S9 in the Supporting Information). Hence, in the experimental system, while the charge from quaternized groups is only $f_{\rm q}$ = 0.04 the charge fraction from protonation of the vinyl groups may be much higher.

Like the block copolymer, the homopolymer penetrates more into the aqueous phase as the charge fraction increases, but with much more sensitivity to the charge fraction. In consequence, the polymer "breaks" the interface as the charge fraction increases. A broader penetration into the aqueous phase and a higher polymer adsorption, as the polymer charge increases, imply a larger decrease of the interfacial tension which is in line with our experimental measurements (see Figure 3).

We now simulate the polymer dissolved in the chloroform phase to investigate the structure of the nonadsorbed polymers during the experimental measurements. The simulations are performed at a constant polymer density of 0.006 molecules/nm³ (see the Methods and Materials section). In the chloroform phase the polymers self-assemble into aggregates of different size and shape depending on the polymer charge fraction, $f_{\bf q}$. Generally, the hydrophilic blocks form a hydrophilic core while the hydrophobic segments extend outward from the hydrophilic core. Figure 8 shows representative structures of the polymer aggregates in chloroform at different charge fractions. Figure 8a shows the uncharged hydrophilic

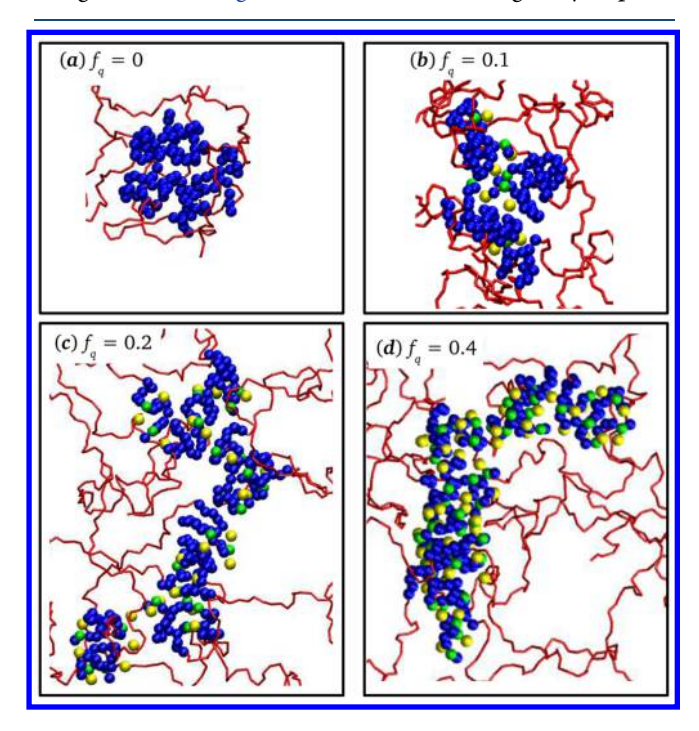


Figure 8. Typical configurations of the homopolymer aggregates in bulk chloroform at charge fractions of (a) $f_{\rm q}=0~(N_{\rm q^2vp}=0)$, (b) $f_{\rm q}=0.1~(N_{\rm q^2vp}=1)$, (c) $f_{\rm q}=0.2~(N_{\rm q^2vp}=2)$, and (d) $f_{\rm q}=0.4~(N_{\rm q^2vp}=4)$. The polymers are initially dispersed in the chloroform at a density of $\rho_s=0.006$ molecules/nm³. The polar groups and the quaternized groups in the hydrophilic block are in dark blue and green, respectively. The counterions are colored in yellow. The hydrophobic backbone groups from the PS block are represented by red sticks. The hydrophobic ring groups are not shown for clarity. $f_{\rm a}=0.16~(N_{\rm hp}=10)$.

blocks forming spherical aggregates. From the lowest charge fraction of $f_q = 0.1$ the electrostatic correlations between the charged groups and counterions break the aggregate's spherical symmetry (see Figure 8b). In Figure 8c the polymer charge fraction is 0.2, and the charged segments stack to form short elongated aggregates. In Figure 8d the charged hydrophilic segments stack to form a helical structure of cylindrical shape at a polymer charge fraction of 0.4. The polymer aggregates in the bulk chloroform phase resemble the aggregates at the water-chloroform interface. The main difference is the dimensionality of the aggregates; at the interface the aggregates are 2D whereas they are 3D in bulk chloroform. The analysis of the polymer self-assembly in chloroform by increasing the hydrophilic fraction f_a and keeping constant the charge fraction $f_q = 0.2$ shows the formation of a three-dimensional percolated state (Figure S11 in the Supporting Information).

The transference of charged groups from the organic medium to water is largely determined by the solvation energy. We investigate the change in the solvation energy, enthalpy, and entropy by transferring a pair of positive and negative ions from the organic liquid to water (see the Supporting Information). Figure 9 shows the results from our

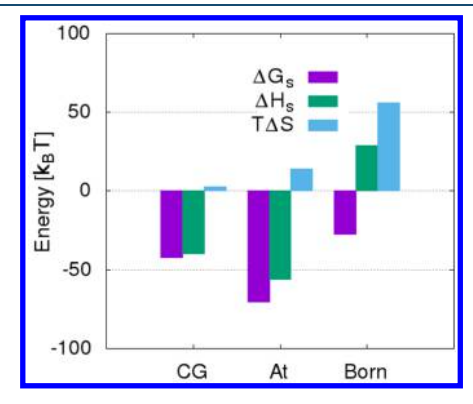


Figure 9. Change in solvation free energy (ΔG_s) , enthalpy (ΔH_s) , and temperature multiplied by the entropy of solvation $(T\Delta S)$ by transferring two charged ions from chloroform to water. The first set of columns are the results from our coarse-grain model (CG); the second set are the results from an atomistic model (At), and the third set are the results from the Born model. The Born model does not agree with the atomistic model while our coarse-grain model qualitatively agrees with it.

coarse-grain model compared with the Born model and an atomistic model. The coarse-grain model and the atomistic model predict that the solvation free energy is mainly of enthalpic origin whereas the Born model requires a large increase of entropy. Both simulation models give qualitatively similar trends of the solvation enthalpy and entropy. The difference between the simulation models could be probably attributed to an underestimation of the hydrogen bonding energy. Ion solvation can be understood by comparing the electrostatic energy between two associated ions in chloroform with the energy when they are solvated in water. The electrostatic potential energy of two associated ions is about $-163k_{\rm B}T$) whereas the potential energy of solvating the two ions each one with four water molecules is about $-270k_{\rm B}T$ (see Figure S13 in the Supporting Information). Interestingly, despite the association in chloroform being very strong the solvation in water is even more favorable.

There is an important entropic contribution when the polymers are adsorbed at the liquid-liquid interface leading to an increase of the accessible volume of the molecules in the liquid phases. This increase of the accessible volume implies an increase of the accessible states of the small molecules meaning an increase the configurational entropy.⁷¹ The main contribution to the increase of entropy is dominated by the volume release from the adsorption of the polymer at the interface. This compensates for the loss of polymer conformational entropy upon adsorption to the interface. The counterion entropy is also important, whose increase is dominated by access to larger configurational states upon dissociation at the interface. However, this entropy gain is diminished at higher charge fractions of the copolymer, when the counterions "condensate" to reduce electrostatic repulsion between the charged copolymer blocks.

Self-assembly driven by electrostatic correlations is observed not only in the chloroform phase but also at the water—chloroform interface at high polymer charge fractions. The effective dielectric constant is higher at the interface than in chloroform which, in turn, gives rise to less negative correlation energies at the interface than in bulk chloroform. At low polymer charge fractions the translational entropy of counterions dominates over the electrostatic correlations leading the counterions to form a diffuse distribution at the interface. Polymer self-assembly driven by electrostatic correlations is observed at high charge fractions when a reduction in the repulsion between quaternized groups at the interface by counterion "condensation" compensates the lost of translational entropy of counterions.

CONCLUSIONS

We have shown that charge fraction along an amphiphilic diblock copolymer and homopolymer can alter the adsorption activity and solution aggregate morphology. We reported that the homopolymer was much more sensitive to the charge fraction than the diblock copolymer, where the hydrophobic tail segment can modulate the adsorption. Using interfacial tension experiments, we have shown that an increase in charge leads to a significantly enhanced adsorption at the chloroform-water interface in both the homopolymer and copolymer cases. Molecular dynamics simulations suggest that this is due to an increased concentration of amphiphiles and the corresponding aggregate morphology at the chloroform-water interface. According to our MD simulations the main polymer and copolymer adsorption mechanisms are (1) the incompatibility between the hydrophilic/hydrophobic groups and the liquid chloroform-water and (2) the solvation energy of charged groups in water. Striking morphological changes of the copolymer assemblies are observed in chloroform and at the water-chloroform interface from the interplay among hydrophilic, hydrophobic, solvation, electrostatic, and entropic contributions. At the interface, as charge increases, the charge-carrying hydrophilic block evolves from spread structures to elongated stripes. When the block copolymers are uncharged, the aggregates spread on the interface to reduce the incompatibility between hydrophilic and hydrophobic groups. At low charge fractions, the aggregates are loosely packed due to the competition between the electrostatic repulsion, hydrophobic association, and counterion dissociation. At higher charge fractions the counterions and the charge groups are strongly correlated to reduce the electrostatic repulsion, resulting in densely packed

aggregates. In chloroform the aggregates of uncharged copolymers are spherical and change into cylindrical helicoids as the charge fraction increases. The charge not only changes interfacial adsorption of these copolymers but can also modulate the self-assembled morphologies in bulk chloroform due to electrostatic correlation driven aggregation. ¹⁸

MATERIALS AND METHODS

Materials. The block copolymer used for this study was a diblock copolymer of polystyrene-block-poly(2-vinylpyridine) (PS-b-P2VP) with molecular weight of 20210 (g/mol) for the PS block and 4220 (g/mol) for the P2VP block and an overall polydispersity index of 1.06. The degree of polymerization is 194 for the PS block, and 40 for the P2VP block. These polymers were synthesized via anionic polymerization by Professor Kenneth R. Shull as reported previously. The molecular weights and polydispersity of the precursor PS block and the final diblock copolymer were confirmed via GPC to ensure that no degradation occurred between synthesis and quaternization.

Quaternized PS-b-P2VP. PS_{194} -b-P2VP $_{40}$ were quaternized at various quaternization ratios. Quaternized diblock copolymers are noted as PS-b-Q2VPyy, where yy is the mole percent of P2VP block that has been quaternized. First, PS₁₉₄-b-P2VP₄₀ were dissolved in DMF (Sigma-Aldrich) at 7 wt %. Ethyl bromide (EtBr, Sigma-Aldrich) of calculated amounts were added to achieve target quaternization ratios. The reaction, shown in Figure 1b, was left to proceed at 40 °C for 120 h and precipitated out into cold diethyl ether (Fisher Scientific) at 1:10 volume ratio. The precipitates were decanted and dried in the vacuum oven at 762 Torr for 8 h, and dialyzed against deionized water for 5 days, with the external solution replaced every 24 h. Purified product was dried and characterized via H¹-NMR, with spectra obtained from a Bruker Avance III 500 MHz system, Ag500. NMR spectra for samples prior to and after quaternization are shown in Figure S1. Degree of quaternization can be determined by the area of peaks at 9.2 ppm, which correspond to the shifts phenolic H in the Q2VP block due to quaternization. The top spectrum corresponds to 37.4% quaternization of the P2VP block. The P2VP homopolymers were quaternized using a similar scheme, and characterized using NMR (Figure S2).

Samples quaternized are summarized in Table 1.

Table 1. Quaternized Versions of PS₁₉₄-b-P2VP₄₀^a

	molecular weight (kg/mol)				
polymer	diblock	PS	Q2VP	$f_{\rm q}$	$W_{\rm Q2VP}/W_{\rm PS\text{-}}b\text{-}\rm Q2VP}$
PS-b-Q2VP0	24.43	20.21	4.22	0	0.173
PS-b-Q2VP4	24.46	20.21	4.25	0.04	0.174
PS-b-Q2VP11	24.54	20.21	4.33	0.11	0.176
PS-b-Q2VP37	24.86	20.21	4.65	0.37	0.187

"The number appended to Q2VP corresponds to the charge percentage $(f_{\rm q})$ in the P2VP block achieved via quaternization.

Interfacial Measurements. Interfacial tension γ of PS-b-Q2VP samples at the chloroform—water interface was measured at room temperature using the drop method, with chloroform (HPLC grade with amylene stabilizers, Sigma-Aldrich, as received) as the embedding phase and Milli-Q water (resistance of 18.2 M Ω cm) as the drop phase. Polymer solutions were prepared at 0.1 mg/mL in chloroform (2.4 \times

 10^{-6} molecules/nm³). This was chosen to be in the dilute regime. Experiments were run inside a glass cuvette (12.5 mm by 22.5 mm by 48 mm) filled with approximately 4 mL of chloroform. By using a U-shaped needle, a drop of water of approximately 4 μ L was created, as shown in Figure 10. A

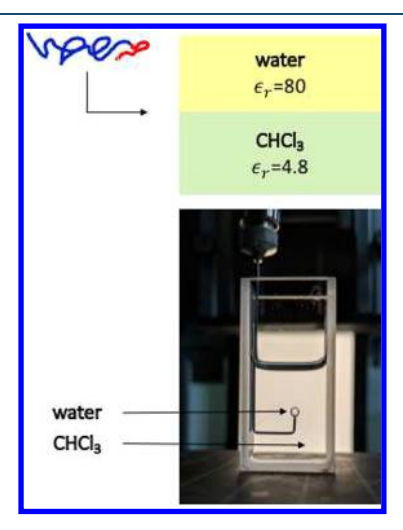


Figure 10. Schematic and photograph of the setup. The two liquid phases have dielectric constants of 80 and 4.4, respectively, which will affect the interfacial adsorption of the block ionomer.

Kruss DSA100 drop shape analyzer stabilized on an active vibration isolating stage was utilized to give γ . The water drop was left to equilibrate with the chloroform phase for 15 min to obtain the baseline interfacial tension of ≈ 32.8 mN/m, which corresponds to the interfacial tension between water and chloroform at room temperature. At 15 min, ≈ 0.2 mL of the polymer solution was injected into the embedding phase. Between runs, the cuvette was thoroughly washed with acetone, ethanol, dichloroethane, and chloroform. Syringe and needle were washed with acetone, ethanol, and Milli-Q water. The experiment was discarded, and the whole cleaning procedure was repeated at the slightest indication of contamination.

Molecular Dynamics. We simulate the adsorption of the PS-*b*-P2VP block copolymer at the water—chloroform interface. We perform molecular dynamics (MD) simulations using a coarse-grain scheme to reduce the total number of degrees of freedom in the system. In the coarse-grain scheme, a group of atoms is modeled by a single particle. The interactions in our system are represented using the Martini force-field. The short-range nonbonded interactions are considered by means of the Lennard-Jones potential

$$u_{ij}^{LJ}(r) = 4\epsilon_{ij} \left[\left(\frac{\sigma_{ij}}{r} \right)^{12} - \left(\frac{\sigma_{ij}}{r} \right)^{6} \right]$$
(3)

where σ_{ij} and ϵ_{ij} are the force-field parameters. The electrostatic interactions are modeled using the Coulomb potential, given by

$$u_{ij}^{\text{el}}(r) = \frac{q_i q_j}{4\pi\epsilon_0 \epsilon_r r} \tag{4}$$

where q_i and q_j are the particles charges, ϵ_0 is the vacuum permittivity, and ϵ_r is the dielectric constant assumed to be equal to 2.5. The particles' type is designated using the notation from the Martini force-field^{61,62} which have

associated values of the Lennard-Jones parameters. The chloroform molecule is represented by a particle of type C4. Water is represented by means of the Martini polarizable model where four water molecules are mapped into a molecule made of three bonded particles making an angle θ (see Figure 4a). The effective dielectric constant of water in the bulk calculated using the polarizable Martini model is $\epsilon_{\rm eff}\approx$ 80, in agreement with the experimental value. The P_4 beads in the coarse-grain model of 2VP are selected by matching the solubility in water (see the Supporting Information).

We simulate diblock PS-b-P2VP block copolymers and quaternized P2VP homopolymers. A copolymer chain consists of two blocks designated as hydrophobic and hydrophilic. The hydrophobic block is formed by $N_{\rm s}$ styrene (nonpolar) monomers, and the hydrophilic one is constituted by $N_{\rm hp}$ monomers; $N_{\rm hp} = N_{\rm 2vp} + N_{\rm q2vp}$ where $N_{\rm 2vp}$ and $N_{\rm q2vp}$ are the number of 2-vinylpyridine (polar) and quaternized (charged) 2-vinylpyridine monomers, respectively. The degree of polymerization is $N_{\rm p} = N_{\rm s} + N_{\rm hp}$. The $N_{\rm q2vp}$ charges from quaternization are distributed randomly in the hydrophilic block. The hydrophilic fraction is calculated as $f_{\rm a} = N_{\rm hp}/N_{\rm p}$ whereas the charge fraction is calculated with respect to number of hydrophilic monomers as $f_{\rm q} = N_{\rm q2vp}/N_{\rm hp}$. In a fully hydrophilic homopolymer $N_{\rm hp} = N_{\rm p}$ implying $f_{\rm a} = 1$ whereas $N_{\rm hp} = 0$ and $f_{\rm a} = 0$ in a fully nonpolar homopolymer.

The atomic and coarse-grain structures of PS-b-P2VP block are shown in Figure 4b. Polystyrene is constituted by a hydrocarbon backbone of CH-CH2 groups and an aromatic ring is hanging from the CH group. The coarse-grain model of polystyrene consists of four particles; the two CH-CH₂ backbone groups are modeled by one particle (1), and the aromatic ring is represented by three particles (2-4, see Figure 4b). The backbone particle is assumed to be of type SCY whereas the ring particles are of type STY (following the notation from the Martini force-field^{61,62}). Particle 1 of the ring is bonded to two neighbor backbone particles. 2-Vinylpyridine is built from styrene by replacing the second CH group in the aromatic ring by a nitrogen atom. This substitution makes polar the 2-vinylpyridine monomer.⁷³ In the coarse-grain model of 2-vinylpyridine, particles 1 and 2 are assumed of type P₄ (polar) whereas particles 3 and 4 are of type STY, like in styrene. Using this parametrization, the partition coefficient (solubility) of the monomer in water calculated from our MD simulations is in good agreement with the experimental measurements (see the Supporting Information). In the quaternized 2-vinylpyridine, particle 1 is of type P₄, and particle 2 is of type Q_a and has a positive unit elementary charge; particles 3 and 4 are of type STY. A free negative counterion is added per Qa particle to maintain electroneutrality.

The simulation setup is shown in Figure 4d and consists of a liquid—liquid interface formed by water and chloroform. One interface forms in the box, and a second interface forms at the edges of the simulation box due to the periodic boundary condition in the z-direction. In the initial configuration a layer of block copolymers is placed at each interface equally spaced on the xy-plane. The box dimensions are $L_x = L_y = 20$ nm, and $L_z \approx 90$ nm along the x-, y-, and z-directions, respectively. The aqueous phase is formed by 82 000 water molecules and spans about 25 nm along the z-direction. The chloroform phase is formed by 2×10^5 particles. The total number of polymers in our simulations is varied from 4 to 200. The polymer surface concentration ranges from 0.001 to 0.23 molecules/nm² (see

DOI: 10.1021/acscentsci.9b00084 ACS Cent. Sci. XXXX, XXX, XXX—XXX

Figure S6). The polymer concentration in the bulk chloroform is less than 0.001 molecules/nm³. In the simulations of a single homopolymer we employed a simulation box of dimensions $L_x = L_y = 12.5$ nm, and $L_z \approx 29$ nm. The chloroform and the water phases are formed by 12 000 and 24 000 molecules, respectively.

The polymer aggregation in bulk chloroform is simulated using a simulation box containing 244 polymer molecules and 2.88×10^5 chloroform particles; the number of counterions is adjusted accordingly with the polymer charge fraction f_q . The simulation box dimensions are $L_x = 32.2$ nm, $L_y = 35$ nm, and $L_z = 35.7$ nm in the x-, y-, and z-directions, respectively.

Our simulation protocol consists of a 50 ns run to thermalize the system at $P_z = 1$ atm and T = 298 K; in this step we use the Berendsen thermostat ($\tau_T = 0.1 \text{ ps}$) and barostat ($\tau_P = 0.5 \text{ ps}$). The equilibration—production run is performed at $P_z = 1$ atm and T = 298 K for at least 500 ns and up to 1 μ s in some cases. In the production runs we used the velocity scale thermostat and Berendsen barostat. After the first equilibration the system is simulated at 350 K for 100 ns and re-equilibrated at T = 298K. No further changes are observed with respect to the first equilibration run. A time-step of 10 fs is used to integrate Newton's equation of motion. Short-range interactions are truncated at 1.3 nm, and long-range electrostatic interactions are computed using the smooth particle mesh Ewald summation. Three-dimensional periodic boundary conditions are applied. The simulations are performed using the open source code GROMACS.^{74–76}

ASSOCIATED CONTENT

S Supporting Information

The Supporting Information is available free of charge on the ACS Publications website at DOI: 10.1021/acscents-ci.9b00084.

NMR spectra, Martini potentials, model calibration method, additional data on copolymer and homopolymer adsorption, and solvation energy calculation methods (PDF)

Movie S1: simulation of a single partially quaternized homopolymer P2VP (randomly charged) at the water-chloroform interface (MPG)

AUTHOR INFORMATION

Corresponding Author

*E-mail: m-olvera@northwestern.edu. Phone: (847) 491-7801.

ORCID ®

Felipe Jiménez-Ángeles: 0000-0001-9473-6892 Ha-Kyung Kwon: 0000-0002-9351-4806

Kazi Sadman: 0000-0003-2872-752X Kenneth R. Shull: 0000-0002-8027-900X

Monica Olvera de la Cruz: 0000-0002-9802-3627

Author Contributions

[⊥]F.J.-A. and H.-K.K. are first authors.

Notes

Safety statement: no unexpected or unusually high safety hazards were encountered.

The authors declare no competing financial interest.

ACKNOWLEDGMENTS

The authors thank Yaoyao Chen for NMR analysis and helpful discussions regarding experimental details. This work was

performed under the financial assistance award 70NANB19H005 from the U.S. Department of Commerce, National Institute of Standards and Technology as part of the Center for Hierarchical Materials Design (CHiMaD). This work was supported by the Sherman Fairchild Foundation.

REFERENCES

- (1) Kim, H.-C.; Park, S.-M.; Hinsberg, W. D. Block Copolymer Based Nanostructures: Materials, Processes, and Applications to Electronics. *Chem. Rev.* **2010**, *110*, 146–177.
- (2) Baba, A.; Locklin, J.; Xu, R.; Advincula, R. Nanopatterning and Nanocharge Writing in Layer-by-Layer Quinquethiophene/Phthalocyanine Ultrathin Films. *J. Phys. Chem. B* **2006**, *110*, 42–45.
- (3) Krishnamoorthy, S.; Pugin, R.; Brugger, J.; Heinzelmann, H.; Hoogerwerf, A. C.; Hinderling, C. Block Copolymer Micelles as Switchable Templates for Nanofabrication. *Langmuir* **2006**, 22, 3450–3452.
- (4) Khanna, V. K. Bottom-up Nanofabrication. In *Integrated Nanoelectronics*. NanoScience and Technology; Springer: New Delhi, 2016
- (5) Kim, S. Y.; Gwyther, J.; Manners, I.; Chaikin, P. M.; Register, R. A. Metal-Containing Block Copolymer Thin Films YieldWire Grid Polarizers with High Aspect Ratio. *Adv. Mater.* **2014**, *26*, 791–795.
- (6) Song, L.; Lam, Y. M. Nanopattern Formation Using a Chemically Modified PS-P4VP Diblock Copolymer. *Nanotechnology* **2007**, *18*, No. 075304.
- (7) Sohn, B.-H.; Yoo, S.-I.; Seo, B.-W.; Yun, S.-H.; Park, S.-M. Nanopatterns by Free-Standing Monolayer Films of Diblock Copolymer Micelles with in Situ Core- Corona Inversion. *J. Am. Chem. Soc.* **2001**, 123, 12734–12735.
- (8) Alvarez, F.; Flores, E.; Castro, L.; Hernández, J.; López, A.; Vazquez, F. Dissipative Particle Dynamics (DPD) Study of Crude Oil-Water Emulsions in the Presence of a Functionalized Co-polymer. *Energy Fuels* **2011**, *25*, 562–567.
- (9) Cendejas, G.; Arreguín, F.; Castro, L. V.; Flores, E. A.; Vazquez, F. Demulsifying Super-Heavy Crude Oil with Bifunctionalized Block Copolymers. *Fuel* **2013**, *103*, 356–363.
- (10) Hernández, E.; Castro-Sotelo, L.; Avendaño Gomez, J.; Flores, C.; Alvarez-Ramirez, F.; Vázquez, F. Synthesis, Characterization, and Evaluation of Petroleum Demulsifiers of Multibranched Block Copolymers. *Energy Fuels* **2016**, *30*, 5363–5378.
- (11) Venkataraman, S.; Hedrick, J. L.; Ong, Z. Y.; Yang, C.; Ee, P. L. R.; Hammond, P. T.; Yang, Y. Y. The effects of polymeric nanostructure shape on drug delivery. *Adv. Drug Delivery Rev.* **2011**, 63, 1228–1246.
- (12) Nguyen, T. D.; Qiao, B.; de la Cruz, M. O. Efficient Encapsulation of Proteins with Random Copolymers. *Proc. Natl. Acad. Sci. U. S. A.* **2018**, *115*, 6578–6583.
- (13) Panganiban, B.; Qiao, B.; Jiang, T.; DelRe, C.; Obadia, M. M.; Nguyen, T. D.; Smith, A. A. A.; Hall, A.; Sit, I.; Crosby, M. G.; Dennis, P. B.; Drockenmuller, E.; Olvera de la Cruz, M.; Xu, T. Random Heteropolymers Preserve Protein Function in Foreign Environments. *Science* **2018**, *359*, 1239–1243.
- (14) Olvera de la Cruz, M.; Belloni, L.; Delsanti, M.; Dalbiez, J. P.; Spalla, O.; Drifford, M. Precipitation of Highly Charged Polyelectrolyte Solutions in the Presence of Multivalent Salts. *J. Chem. Phys.* **1995**, *103*, 5781–5791.
- (15) Priftis, D.; Xia, X.; Margossian, K. O.; Perry, S. L.; Leon, L.; Qin, J.; de Pablo, J. J.; Tirrell, M. Ternary, Tunable Polyelectrolyte Complex Fluids Driven by Complex Coacervation. *Macromolecules* **2014**, *47*, 3076–3085.
- (16) Borisov, O. V.; Zhulina, E. B. Morphology of Micelles Formed by Diblock Copolymer with a Polyelectrolyte Block. *Macromolecules* **2003**, *36*, 10029–10036.
- (17) Huang, C.; de la Cruz, M. O.; Swift, B. W. Phase Separation of Ternary Mixtures: Symmetric Polymer Blends. *Macromolecules* **1995**, 28, 7996–8005.

(18) Ma, B.; Nguyen, T. D.; Pryamitsyn, V. A.; Olvera de la Cruz, M. Ionic Correlations in Random Ionomers. *ACS Nano* **2018**, *12*, 2311–2318.

- (19) Bolintineanu, D. S.; Stevens, M. J.; Frischknecht, A. L. Atomistic Simulations Predict a Surprising Variety of Morphologies in Precise Ionomers. *ACS Macro Lett.* **2013**, *2*, 206–210.
- (20) Hall, L. M.; Seitz, M. E.; Winey, K. I.; Opper, K. L.; Wagener, K. B.; Stevens, M. J.; Frischknecht, A. L. Ionic Aggregate Structure in Ionomer Melts: Effect of Molecular Architecture on Aggregates and the Ionomer Peak. *J. Am. Chem. Soc.* **2012**, *134*, 574–587.
- (21) Middleton, L. R.; Winey, K. I. Nanoscale Aggregation in Acidand Ion-Containing Polymers. *Annu. Rev. Chem. Biomol. Eng.* **2017**, *8*, 499–523.
- (22) Appetecchi, G. B.; Kim, G.-T.; Montanino, M.; Alessandrini, F.; Passerini, S. Room Temperature Lithium Polymer Batteries Based on Ionic Liquids. *J. Power Sources* **2011**, *196*, 6703–6709.
- (23) Park, M. J.; Balsara, N. P. Phase Behavior of Symmetric Sulfonated Block Copolymers. *Macromolecules* **2008**, *41*, 3678–3687.
- (24) Rojas, A. A.; Inceoglu, S.; Mackay, N. G.; Thelen, J. L.; Devaux, D.; Stone, G. M.; Balsara, N. P. Effect of Lithium-Ion Concentration on Morphology and Ion Transport in Single-Ion-Conducting Block Copolymer Electrolytes. *Macromolecules* **2015**, 48, 6589–6595.
- (25) Sing, C. E.; Zwanikken, J. W.; Olvera de la Cruz, M. Electrostatic Control of Block Copolymer Morphology. *Nat. Mater.* **2014**, *13*, 694–698.
- (26) Zwanikken, J. W.; Jha, P. K.; de la Cruz, M. O. A practical Integral Equation for the Structure and Thermodynamics of Hard Sphere Coulomb Fluids. *J. Chem. Phys.* **2011**, *135*, No. 064106.
- (27) Kwon, H.-K.; Zwanikken, J. W.; Shull, K. R.; Olvera de la Cruz, M. Theoretical Analysis of Multiple Phase Coexistence in Polyelectrolyte Blends. *Macromolecules* **2015**, *48*, 6008–6015.
- (28) Kwon, H.-K.; Pryamitsyn, V. A.; Zwanikken, J. W.; Shull, K. R.; Olvera de la Cruz, M. Solubility and Interfacial Segregation of Salts in Ternary Polyelectrolyte Blends. *Soft Matter* **2017**, *13*, 4830–4840.
- (29) Pryamitsyn, V. A.; Kwon, H.-K.; Zwanikken, J. W.; Olvera de La Cruz, M. Anomalous Phase Behavior of Ionic Polymer Blends and Ionic Copolymers. *Macromolecules* **2017**, *50*, 5194–5207.
- (30) Wang, Z.-G. Effects of Ion Solvation on the Miscibility of Binary Polymer Blends. *J. Phys. Chem. B* **2008**, *112*, 16205–16213.
- (31) Wang, Z.-G. Fluctuation in Electrolyte Solutions: The Self Energy. *Phys. Rev. E* **2010**, *81*, No. 021501.
- (32) Nakamura, I.; Wang, Z.-G. Thermodynamics of Salt-Doped Block Copolymers. ACS Macro Lett. 2014, 3, 708–711.
- (33) Hou, K. J.; Qin, J. Solvation and Entropic Regimes in Ion-Containing Block Copolymers. *Macromolecules* **2018**, *51*, 7463–7475.
- (34) Cox, J. K.; Yu, K.; Eisenberg, A.; Bruce Lennox, R. Compression of polystyrenepoly(ethylene oxide) surface aggregates at the air/water interface. *Phys. Chem. Chem. Phys.* **1999**, *1*, 4417–4421.
- (35) Zhu, J.; Eisenberg, A.; Lennox, R. B. Interfacial behavior of block polyelectrolytes. 5. Effect of varying block lengths on the properties of surface micelles. *Macromolecules* **1992**, 25, 6547–6555.
- (36) Gonçalves da Silva, A. M.; Simões Gamboa, A. L.; Martinho, J. M. G. Aggregation of Poly(styrene)Poly(ethylene oxide) Diblock Copolymer Monolayers at the AirWater Interface. *Langmuir* **1998**, *14*, 5327–5330.
- (37) Zhu, J.; Eisenberg, A.; Lennox, R. B. Interfacial Behavior of Block Polyelectrolytes. 1. Evidence for Novel Surface Micelle Formation. *J. Am. Chem. Soc.* **1991**, *113*, 5583–5588.
- (38) Cheyne, R. B.; Moffitt, M. G. Self-Assembly of Polystyrene-block-Poly (Ethylene Oxide) Copolymers at the Air- Water Interface: Is Dewetting the Genesis of Surface Aggregate Formation? *Langmuir* **2006**, 22, 8387–8396.
- (39) Chung, B.; Choi, M.; Ree, M.; Jung, J. C.; Zin, W. C.; Chang, T. Subphase pH Effect on Surface Micelle of Polystyrene-b-poly(2-vinylpyridine) Diblock Copolymers at the Air—Water Interface. *Macromolecules* **2006**, *39*, 684–689.
- (40) Chung, B.; Choi, H.; Park, H.-W.; Ree, M.; Jung, J. C.; Zin, W. C.; Chang, T. Mixed Surface Micelles of Polystyrene-b-poly(2-

vinylpyridine) and Polystyrene-b-poly(methyl methacrylate). *Macromolecules* **2008**, *41*, 1760–1765.

- (41) Baker, S.; Leach, K.; Devereaux, C.; Gragson, D. Controlled Patterning of Diblock Copolymers by Monolayer Langmuir-Blodgett Deposition. *Macromolecules* **2000**, *33*, 5432–5436.
- (42) Claro, P. C. d. S.; Coustet, M. E.; Diaz, C.; Maza, E.; Cortizo, M. S.; Requejo, F. G.; Pietrasanta, L. I.; Ceoln, M.; Azzaroni, O. Selfassembly of PBzMA-b-PDMAEMA Diblock Copolymer Films at the AirWater Interface and Deposition on Solid Substrates Via LangmuirBlodgett Transfer. *Soft Matter* **2013**, *9*, 10899–10912.
- (43) Seo, Y.-S.; Kim, K. S.; Galambos, A.; Lammertink, R. G. H.; Vancso, G. J.; Sokolov, J.; Rafailovich, M. Nanowire and Mesh Conformations of Diblock Copolymer Blends at the Air/Water Interface. *Nano Lett.* **2004**, *4*, 483–486.
- (44) Richard-Lacroix, M.; Borozenko, K.; Pellerin, C.; Bazuin, C. G. Bridging the Gap between the Mesoscopic 2D Order—Order Transition and Molecular-Level Reorganization in Dot-Patterned Block Copolymer Monolayers. *Macromolecules* **2016**, *49*, 9089—9099.
- (45) Lu, Q.; Bazuin, C. G. Solvent-Assisted Formation of Nanostrand Networks from Supramolecular Diblock Copolymer/Surfactant Complexes at the Air/Water Interface. *Nano Lett.* **2005**, *S*, 1309–1314.
- (46) Perepichka, I. I.; Borozenko, K.; Badia, A.; Bazuin, C. G. Pressure-Induced Order Transition in Nanodot-Forming Diblock Copolymers at the Air/Water Interface. *J. Am. Chem. Soc.* **2011**, *133*, 19702–19705.
- (47) Kim, D. H.; Kim, S. Y. Effective Morphology Control of Block Copolymers and Spreading Area-Dependent Phase Diagram at the Air/Water Interface. *J. Phys. Chem. Lett.* **2017**, *8*, 1865–1871.
- (48) Lu, H.; Lee, D. H.; Russell, T. P. Temperature Tunable Micellization of Polystyrene-blockpoly (2-vinylpyridine) at Si- Ionic Liquid Interface. *Langmuir* **2010**, *26*, 17126–17132.
- (49) Perepichka, I. I.; Lu, Q.; Badia, A.; Bazuin, C. G. Understanding and Controlling Morphology Formation in Langmuir—Blodgett Block Copolymer Films Using PS-P4VP and PSP4VP/PDP. *Langmuir* **2013**, 29, 4502—4519.
- (50) Shi, L.; Tummala, N. R.; Striolo, A. C₁₂E₆ and SDS Surfactants Simulated at the Vacuum–Water Interface. *Langmuir* **2010**, 26, 5462–5474.
- (51) Yazhgur, P.; Vierros, S.; Hannoy, D.; Sammalkorpi, M.; Salonen, A. Surfactant Interactions and Organization at the Gas—Water Interface (CTAB with Added Salt). *Langmuir* **2018**, *34*, 1855—1864.
- (52) Xue, Y.; He, L.; Middelberg, A. P. J.; Mark, A. E.; Poger, D. Determining the Structure of Interfacial Peptide Films: Comparing Neutron Reflectometry and Molecular Dynamics Simulations. *Langmuir* **2014**, *30*, 10080–10089.
- (53) Jiménez-Ángeles, F.; Firoozabadi, A. Tunable Substrate Wettability by Thin Water Layer. J. Phys. Chem. C 2016, 120, 24688–24696.
- (54) Jiménez-Ángeles, F.; Khoshnood, A.; Firoozabadi, A. Molecular Dynamics Simulation of the Adsorption and Aggregation of Ionic Surfactants at Liquid–Solid Interfaces. *J. Phys. Chem. C* **2017**, *121*, 25908–25920.
- (55) Jiménez-Ángeles, F.; Firoozabadi, A. Hydrophobic Hydration and the Effect of NaCl Salt in the Adsorption of Hydrocarbons and Surfactants on Clathrate Hydrates. *ACS Cent. Sci.* **2018**, *4*, 820–831.
- (56) Bui, T.; Phan, A.; Monteiro, D.; Lan, Q.; Ceglio, M.; Acosta, E.; Krishnamurthy, P.; Striolo, A. Evidence of Structure-Performance Relation for Surfactants Used as Antiagglomerants for Hydrate Management. *Langmuir* **2017**, *33*, 2263–2274.
- (57) Ndao, M.; Goujon, F.; Ghoufi, A.; Malfreyt, P. Coarse-grained modeling of the oil-water-surfactant interface through the local definition of the pressure tensor and interfacial tension. *Theor. Chem. Acc.* **2017**, *136*, 21.
- (58) Ruiz-Morales, Y.; Romero-Martínez, A. Coarse-Grain Molecular Dynamics Simulations To Investigate the Bulk Viscosity and Critical Micelle Concentration of the Ionic Surfactant Sodium

Dodecyl Sulfate (SDS) in Aqueous Solution. J. Phys. Chem. B 2018, 122, 3931–3943.

- (59) Marrink, S. J.; Risselada, H. J.; Yefimov, S.; Tieleman, D. P.; de Vries, A. H. The MARTINI Force Field: Coarse Grained Model for Biomolecular Simulations. *J. Phys. Chem. B* **2007**, *111*, 7812–7824.
- (60) Yesylevskyy, S. O.; Schäfer, L. V.; Sengupta, D.; Marrink, S. J. Polarizable Water Model for the Coarse-Grained MARTINI Force Field. *PLoS Comput. Biol.* **2010**, *6*, 1–17.
- (61) Rossi, G.; Monticelli, L.; Puisto, S. R.; Vattulainen, I.; Ala-Nissila, T. Coarse-Graining Polymers with the MARTINI Force-Field: Polystyrene as a Benchmark Case. *Soft Matter* **2011**, *7*, 698–708.
- (62) Vögele, M.; Holm, C.; Smiatek, J. Coarse-grained simulations of polyelectrolyte complexes: MARTINI models for poly(styrene sulfonate) and poly(diallyldimethylammonium). *J. Chem. Phys.* **2015**, *143*, 243151.
- (63) Adamson, A. W.; Gast, A. P. Physical Chemistry of Surfaces; Interscience publishers, 1967.
- (64) Carvajal, D.; Laprade, E. J.; Henderson, K. J.; Shull, K. R. Mechanics of Pendant Drops and Axisymmetric Membranes. *Soft Matter* **2011**, *7*, 10508–10519.
- (65) Satoh, M.; Yoda, E.; Hayashi, T.; Komiyama, J. Potentiometric Titration of Poly(Vinylpyridines) and Hydrophobic Interaction in the Counterion Binding. *Macromolecules* 1989, 22, 1808–1812.
- (66) Ndao, M.; Devmy, J.; Ghoufi, A.; Malfreyt, P. Coarse-Graining the LiquidLiquid Interfaces with the MARTINI Force Field: How Is the Interfacial Tension Reproduced? *J. Chem. Theory Comput.* **2015**, 11, 3818–3828.
- (67) Pimenova, N.; Afanas'ev, V.; Davydova, O.; Krestov, G. Dielectric Constant Measurement in Nonaqueous Systems on the Basis of Acetone. *Izv. Vyssh. Uchebn. Zaved. Khim. Khim. Tekhnol.* **1984**, 27, 1043–1045.
- (68) Archer, D. G.; Wang, P. The Dielectric Constant of Water and DebyeHckel Limiting Law Slopes. *J. Phys. Chem. Ref. Data* **1990**, *19*, 371–411.
- (69) Deserno, M.; Jiménez-Ángeles, F.; Holm, C.; Lozada-Cassou, M. Overcharging of DNA in the Presence of Salt: Theory and Simulation. J. Phys. Chem. B 2001, 105, 10983–10991.
- (70) Deiss-Yehiely, E.; Ortony, J. H.; Qiao, B.; Stupp, S. I.; Olvera de la Cruz, M. Ion Condensation onto Self-assembled Nanofibers. *J. Polym. Sci., Part B: Polym. Phys.* **2017**, *55*, 901–906.
- (71) Jiménez-Ángeles, F.; Lozada-Cassou, M. A Model Macroion Solution Next to a Charged Wall: Overcharging, Charge Reversal, and Charge Inversion by Macroions. *J. Phys. Chem. B* **2004**, *108*, 7286–7296
- (72) Shull, K. R.; Kramer, E. J.; Hadziioannou, G.; Tang, W. Segregation of Block Copolymers to Interfaces Between Immiscible Homopolymers. *Macromolecules* **1990**, 23, 4780–4787.
- (73) Rowbotham, J. B.; Schaefer, T. Long-range ProtonProton Coupling Constants in the Vinylpyridines. Conformational Preferences of the Vinyl Group and Molecular Orbital Calculations. *Can. J. Chem.* **1974**, *52*, 136–142.
- (74) Berendsen, H.; Spoel, D. V. D.; Drunen, R. V. Gromacs: A Message-Passing Parallel Molecular Dynamics Implementation. *Comput. Phys. Commun.* **1995**, *91*, 43–56.
- (75) Van Der Spoel, D.; Lindahl, E.; Hess, B.; Groenhof, G.; Mark, A. E.; Berendsen, H. J. C. GROMACS: Fast, Flexible, and Free. *J. Comput. Chem.* **2005**, *26*, 1701–1718.
- (76) Hess, B.; Kuttner, C.; van der Spoel, D.; Lindahl, E. GROMACS 4: Algorithms for Highly Efficient, Load-Balanced, and Scalable Molecular Simulation. J. Chem. Theory Comput. 2008, 4, 435–447.